Wind and Structures, *Vol. 29, No. 6 (2019) 405-416*
DOI: https://doi.org/10.12989/was.2019.29.6.405

Validation of the numerical simulations of flow around a scaled-down turbine using experimental data from wind tunnel

M. Salman Siddiqui*[1], Adil Rasheed[2a] and Trond Kvamsdal[1b]

[1]*Department of Mathematical Sciences, Norwegian University of Science and Technology, NO-7491 Trondheim, Norway*
[2]*Department of Mathematics and Cybernetics, SINTEF Digital, NO-7465 Trondheim, Norway*

(Received February 5, 2019, Revised June 25, 2019, Accepted July 10, 2019)

Abstract. Aerodynamic characteristic of a small scale wind turbine under the influence of an incoming uniform wind field is studied using k-ω Shear Stress Transport turbulence model. Firstly, the lift and drag characteristics of the blade section consisting of S826 airfoil is studied using 2D simulations at a Reynolds number of 1×10^5. After that, the full turbine including the rotational effects of the blade is simulated using Multiple Reference Frames (MRF) and Sliding Mesh Interface (SMI) numerical techniques. The differences between the two techniques are quantified. It is then followed by a detailed comparison of the turbine's power/thrust output and the associated wake development at three tip speeds ratios (λ = 3, 6, 10). The phenomenon of blockage effect and spatial features of the flow are explained and linked to the turbines power output. Validation of wake profiles patterns at multiple locations downstream is also performed at each λ. The present work aims to evaluate the potential of the numerical methods in reproducing wind tunnel experimental results such that the method can be applied to full-scale turbines operating under realistic conditions in which observation data is scarce or lacking.

Keywords: wind energy; aerodynamics; wind tunnel tests; computational fluid dynamics; high fidelity simulations

1. Introduction

Modern wind turbines operate under the wake of upstream turbines and experience lower wind magnitudes and higher turbulent intensity as described by Siddiqui *et al.* (2017), Alexandros and Chick (2013), Siddiqui *et al.* (2019). To develop efficient turbine models capable of withstanding the variations in flow; initial preliminary technical assessment is paramount as reported by Krogstad and Saetran (2012). This can not only reduce development costs by providing an accurate estimate of loads under different operating conditions but also minimize the chances of structural failure. The methodologies utilized in the context of wind turbines are either experimental or numerical as explored in Keerthana and Harikrishna (2017). In the former category Sørensen *et al.* (2002) tested a 5 m radius wind turbine inside a closed wind tunnel having a test section of 24 m x 36 m at National Renewable Energy Laboratory (NREL). The wind tunnel test remains a unique test in terms of the sheer size of the model tested. However, due to significant uncertainties linked with the experimental data, the participants did not reach a definite conclusion on the aerodynamic loading and wake development. Another experiment worth mentioning here is the Model Experiments in Controlled Conditions (MEXICO) project conducted by Snel *et al.* (2007) which is aimed at providing a stable and reliable experimental dataset. The experiment involved a turbine with 2.25 m long blades installed inside a wind tunnel with a test section of 9.5 m x 9.5 m. Particle Image Velocimetry (PIV) method was employed to map the flow field quantitatively. Thus the experiment provided not only the aerodynamic characteristics of the wind turbine but also its wake characteristics. One of the latest and detailed experiment campaign by Krogstad *et al.* (2015) was conducted at the Norwegian University of Science and Technology (NTNU). The experiment involved a 0.45 m radius turbine inside a wind tunnel with a dimension of 2.71 m x 1.81 m x 11.15 m. The recorded dataset is available in the form of aerodynamic loads on the structure, wake velocity deficit and turbulent kinetic energy profiles at multiple locations downwind of the turbine over a range of tip speed ratios (λ).

Although experiments like these have advanced our understanding of the wind turbines, they have not helped much in applying the understanding to a full-scale turbine operating under realistic conditions as mentioned by Luhur *et al.* (2016). At this point, the numerical approach comes as an attractive alternative. The first category of these models consists of implicitly simulating turbine behavior using simplified parameterizations. Amongst the modeling techniques available to correctly model and predict the aerodynamic loads on wind turbines structure, methods such as Blade Element Model (BEM) as given by Yang *et al.* (2014), Actuator Disc (AD) as described by Crasto *et al.* (2012) and Actuator Line Methods (ALM) given by Stevens *et al.* (2018), Crespo *et al.* (1999) are deemed efficient. Such methods draw a rapid estimation of the aerodynamic loading on the structure. Analytical vortex models developed by Cleaver *et al.* (2010) are usually coupled with

*Corresponding author, Postdoctoral researcher
E-mail: muhammad.siddiqui@ntnu.no
[a] Senior scientist
E-mail: adil.rasheed@sintef.no
[b] Professor
E-mail: trond.kvamsdal@ntnu.no

http://www.techno-press.com/journals/was&subpage=7
ISSN: 1226-6116 (Print), 1598-6225 (Online)

Table 1 NTNU Blind test: An overview of the geometrical complexity, aerodynamic models, techniques for handling rotational rotor and turbulence model employed in previous and present study of the wind tunnel test performed at NTNU. Previous studies are reported in Krogstad and Eriksen (2013), Sanderse *et al.* (2013), Sørensen *et al.* (2013)

	Geometric modeling			Aerodynamic modeling			Rotor modeling		Turbulence modeling	
Authors	Rotor	Nacelle	Tower	ALM	AD	FR	MRF	SMI	RANS	LES
Lund	X				X			X	X	
Manger	X	X	X			X		X	X	
Hansen	X					X	X		X	
Sørensen	X			X	X					X
Melheim	X				X				X	
Kalvig	X		X		X				X	
Present	X	X	X			X	X	X	X	

BEM to provide an enhanced estimate of the configuration of wake in the downstream direction. Though, on certain occasions, lack of comprehensive visualization of the flow field and numerous assumptions adopted in the development of these models reduce the plausibility of the conclusions. Fully resolved flow simulations where the rotational effects of the rotors are explicitly resolved addresses some of the shortcomings and are gaining popularity thanks to the immense computational power available at our disposal as described in Ilhan *et al.* (2018). Many researchers have utilized the experimental results provided by Sørensen *et al.* (1998), Troldborg *et al.* (2007) to validate their existing simulation models for the predictions related to small wind turbines. J. Kvalvik of Aclona Flow used 120^o rotor sector exploiting axial symmetry to model the turbine rotor. E. Manger also performed a similar numerical investigation, however, with the entire structure using the Sliding Mesh Technique (SMI) on a mesh consisting of 5.3 x 10^6 cells. He employed Fluent (2019) and used k-ω SST turbulence model to perform the simulations. Martinez *et al.* (2015) used actuator line, and Zhong *et al.* (2015) used actuator disk theory to model the rotor and ignored nacelle and tower from the analysis. A brief overview of the most notable numerical investigation of the NTNU turbine is presented in the Table 1. The main contributions of the present work is an inter-comparison of different modeling techniques and a quantitative evaluation of the impact of geometric complexity on the modeling accuracy.

In the current work, high fidelity numerical simulations are conducted using MRF (Multiple Reference Frames), and SMI (Sliding Mesh Interface) techniques and the results are validated against the wind tunnel experimental data by Krogstad and Eriksen (2013). In contrast to most of the other participants in the blind test, the present simulations made minimal geometrical approximations. In other words, the rotating blades, nacelle and tower geometry are explicitly modeled using a RANS approach as described by Li *et al.* (2016) and Ozdogan *et al.* (2017). Before conducting the simulation of the full turbine, the aerodynamic characteristics of the NREL-S826 airfoil over a range of angle of attacks (α) was evaluated and compared to the wind tunnel experiments. The turbine blade consists of the cross-section represented by S826 airfoil. The accuracy of both the simulation techniques (MRF and SMI) is established against the measurements. After that, turbines aerodynamic performance (C_p, C_t) and the wake deficit (1-U/U_{ref}) is assessed over a range of operating conditions (λ of 3, 6, 9).

2. Governing equations

To model the flow around the wind turbine, MRF and SMI numerical modeling techniques are selected. A brief description along with the governing equations are provided in the following subsection.

2.1 Multiple reference frames (MRF)

In this approach, the turbine rotor is made to remain stationary, while source/sink terms (centripetal and centrifugal forces) are added to the systems of governing equations which yields the desired rotational effects. The domain is divided into rotational and stationary zones as described by Jasak (2009). The following momentum and mass conservation equations correspond to the stationary zone:

$$\nabla \cdot (\mathbf{u}_a \otimes \mathbf{u}_a) = -\nabla p + \nabla \cdot (\nu + \nu_t)(\nabla \mathbf{u}_a + (\nabla \mathbf{u}_a)^{\mathrm{T}})$$

$$\nabla \cdot \mathbf{u}_a = 0$$

$\mathbf{u}_a$ represents the absolute velocity as observed from the outside stationary zone. Whereas, inside the rotating region, the equations are written in the form of relative velocity $\mathbf{u}_r$ in the following manner

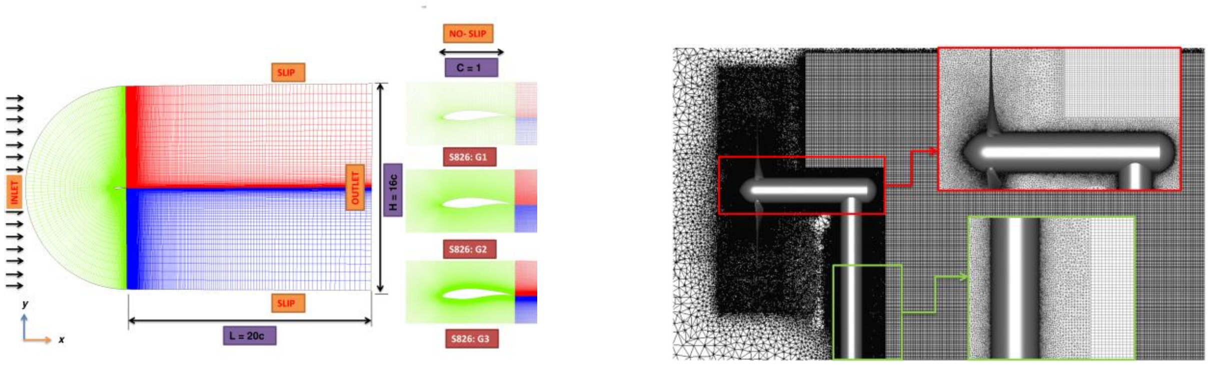

(a) (b)

Fig. 1 Domain and computational mesh for simulation of flow around the (a) S826 airfoil - three different computational meshes ($\mathbb{G}_1$=57800, $\mathbb{G}_2$= 82560, $\mathbb{G}_3$=135540) and boundary conditions for the 2D simulations (b) full 3D rotating turbine with nacelle and support structure (4×10^6 cells)

$$\nabla\cdot(\mathbf{u}_r\otimes\mathbf{u}_r)+2\Omega\times\mathbf{u}_r+\Omega\times(\Omega\times r)=-\nabla p+\nabla\cdot(\nu+\nu_t)(\nabla\mathbf{u}_r+(\nabla\mathbf{u}_r)^{\mathrm{T}})$$
$$\nabla\cdot\mathbf{u}_r=0$$

$$\mathbf{u}_a=\mathbf{u}_r+\Omega\times r$$

In the equation above p, ν and ν_t represent the pressure, kinematic viscosity and turbulent viscosity. The Ω stands for the angular velocity of the rotating zone. MRF solves for the steady state; hence the temporal terms are not accounted for in the governing equations.

2.2 Sliding mesh interface (SMI)

The SMI approach takes into account the dynamic unsteady behavior of the turbine by utilizing the blade and hence the mesh rotation. The mesh region encompassing the rotor physically rotate with every new time step. This method is proven to be computationally expensive by Sanderse *et al.* (2013) but more accurate than other methods. SMI approach requires the following system of equations to be solved. Here $\mathbf{u}$ is the fluid velocity and $\mathbf{u_g}$ is the grid velocity (which is zero for the static part of grid)

$$\frac{\partial\mathbf{u}}{\partial t}+\nabla\cdot((\mathbf{u}-\mathbf{u_g})\otimes\mathbf{u})+\nabla\cdot(\nu+\nu_t)(\nabla\mathbf{u}+(\nabla\mathbf{u})^{\mathrm{T}})-\nabla p=\mathbf{f}$$

$$\nabla\cdot(\mathbf{u}-\mathbf{u_g})=0$$

3. Approach and methods

3.1 Development of CAD model

A CAD model of the turbine is constructed with precise dimensions as per the guidelines provided in the wind tunnel experimental test conducted by Krogstad and Eriksen (2013). The blade's construction is highly stiff with 14% thick S826 airfoil, which was initially developed in NREL by Somers (2005). To endure high structural loading cylindrical cross section is employed at the root of the blades. The test turbine has three blades and a diameter of D = 0.944 m which rotates in a counterclockwise direction. For the ease of mesh generation, the model is formed with smoothened sprockets at the connection of blades and the nacelle to avoid sharp edges which would otherwise require exceptionally higher mesh elements for the resolution at the discretization stage. It is believed that the slight modification would not alter the overall accuracy of the solution, significantly reduce the number of mesh points thereby reducing the computational costs. However, no similar modification is employed near the tip corner regions since it is suspected to be a highly sensitive area aerodynamically. The schematic of the CAD model is presented in Fig. 1(b).

3.2 Domain and mesh

The computational mesh for the two-dimensional S826 airfoil is developed using three sets of mesh grading ($\mathbb{G}_1, \mathbb{G}_2, \mathbb{G}_3$) parameters to achieve mesh independence. The mesh grading of $\mathbb{G}_2$ with 82 560 cells is found to reach the mesh independent state and thus selected for subsequent numerical investigations in two-dimensions. The domain of the present simulation setup (20*c* x 8*c*, where *c* is the airfoil chord length) is selected based on our previously conducted domain independence studies by Nordanger *et al.* (2015). For meshing the complete three-dimensional model, a hybrid meshing strategy is utilized. It consists of highly concentrated tetrahedral cells near the turbine surface to capture sharp gradients, whereas, the computational mesh steadily transitions to bigger cells in the direction of wind tunnel walls. To successfully resolve the small, turbulent structures inside the wake, a region of an extremely refined computational block which extends between x/R = 1.5 to x/R = 7 (R represents the turbine radius) is formed. The present meshing strategy is assumed to help in the validation of the aerodynamic loads on the

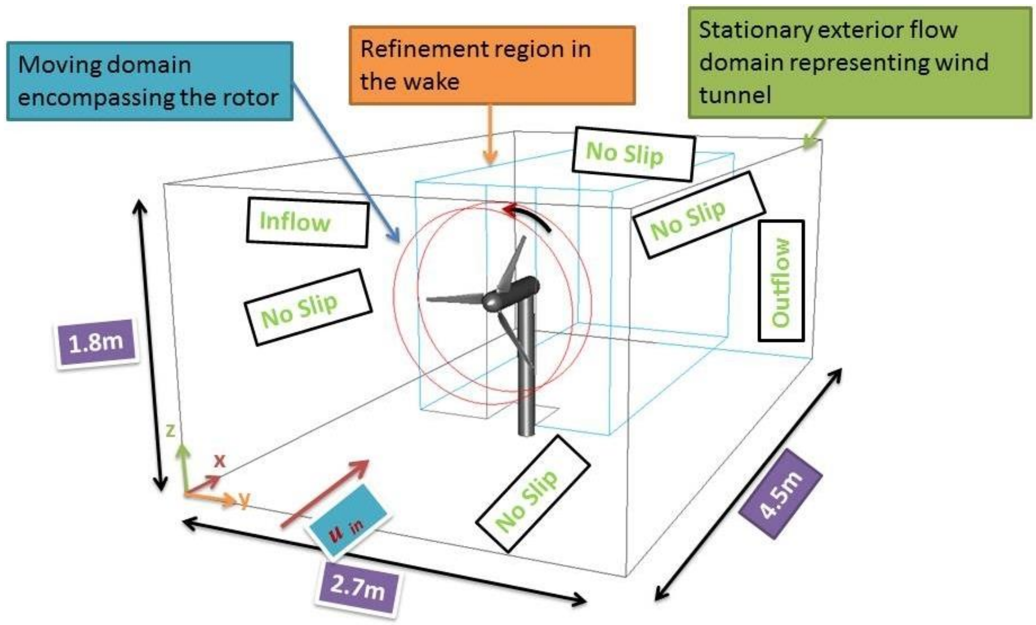

Fig. 2 NTNU Blind Test: Overview of the computational domain and imposed boundary conditions which correspond to the wind tunnel experiments conducted by Krogstad and Eriksen (2013)

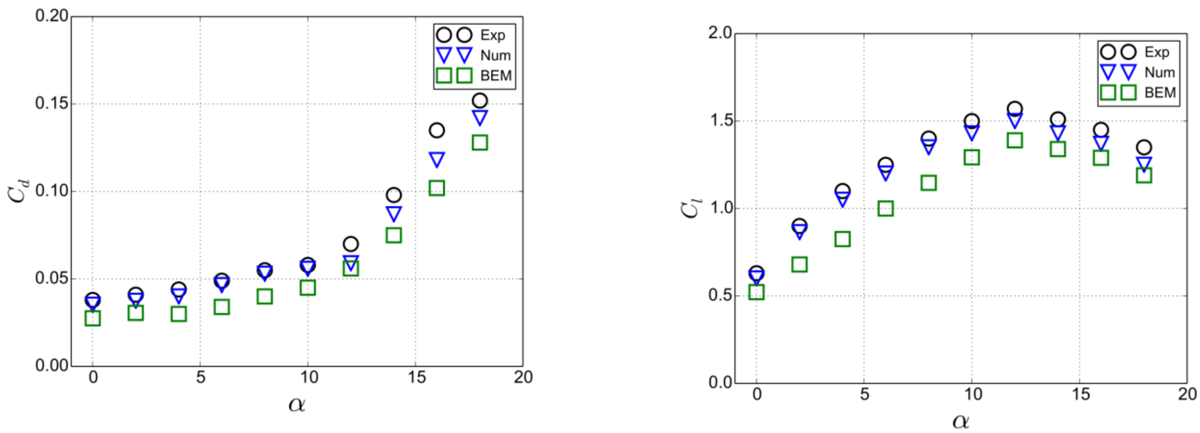

(a) Drag coefficient (b) Lift coefficient

Fig. 3 NREL-S826 airfoil (2D aerodynamics): Our numerically computed (Num) (a) drag and (b) lift coefficients over the range of angles of attack (α) for Re = 1×10^5. The experimental (Exp) and Blade Element Model (BEM) data are provided by Krogstad and Eriksen (2013)

structure in addition to providing an accurate estimate of the wake pattern in the downstream direction. The $y^+ = \frac{u_* y}{\nu}$ (u_* describes the friction velocity at the nearest wall, y is the distance to the most adjacent wall, and ν represents the kinematic viscosity) is maintained in the log-law region, and varied such that it remains between $30 \leq y^+ \leq 100$ so that the wall functions calculate the correct values of the field variables for the neighboring cells adjacent to the wall. The overall mesh size of the computational domain consists of nearly 4×10^6 cells. To develop separate rotational and non-rotational regions, a zonal approach is employed. The stationary zone ($4.5\text{m} \times 2.7\text{m} \times 1.8\text{m}$) represents the wind tunnel and include the turbine nacelle and tower. Whereas, the rotor is located inside the rotating area. A complete schematic diagram of the computational domain is presented in Fig. 2.

3.3 Boundary conditions

The boundary conditions are applied in such a way that they exactly portray the actual wind tunnel conditions. At the inlet, a fixed inlet free stream velocity condition is applied, and the λ of the turbine is modified by changing the

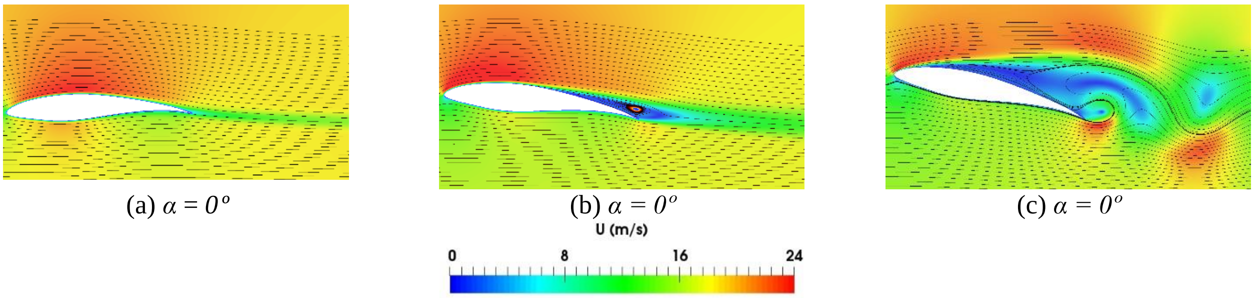

Fig. 4 NREL S826 airfoil (2D aerodynamics): Comparison of flow pattern (velocity contour with super imposed streamlines) over the studied range of angles of attack (α). The plots displays (a) attached flow, (b) mildly separated flow, and (c) severely non-attached flow (stall)

angular speed of the rotor, whereas outflow boundary condition is prescribed at the outlet. To match the inner and outer regions of computational mesh, an interface is developed to match the correct transfer of fluxes across the two regions. No-slip wall condition is applied to the domain walls and the turbine structure as described in Wilcox (1994). Fig. 2 presents the boundary conditions used in the current work.

3.4 Solver settings

The simulations are conducted at the standard conditions as defined in the experimental campaign of the study by Krogstad and Eriksen (2013). The reference flow velocity (U_{ref}) remains at 10 m/s in all the simulations and the rotational speed Ω is varied to achieve the desired λ of 3, 6, 10. The flow is assumed to be incompressible with fixed fluid density $\rho = 1.225$ kg/m ^{3} and the dynamic viscosity $\mu = 1.82 \times 10^{-5}$ kg/m.s, Turbulent kinetic energy (k) and rate of dissipation (ω) are varied until the desired representation of turbulent intensity at the turbine location is achieved. The solver is built in OpenFOAM-4.0 (OF) which is based on a finite volume discretization strategy, which utilizes the divergence theorem to integrate the equations over the control volume. This way the volume integral of the divergence of field variables turns into the surface integrals over faces of the control volume. For the solution of discretized equations, Geometric Agglomerated Algebraic Multigrid (GAMG) solver is used. For the transient simulations, a first order implicit scheme is employed for handling the time-dependent term. The convection term of the Navier-Stokes is discretized using the bounded Gauss upwind. For the solution of the diffusion term, Gauss linear corrector is used. The simulations are run until the convergence criteria is achieved (Residuals $\leq 10^{-6}$).

4. Results and discussion

In this section, a comparison of our numerical methods against the experimental results is presented. The lift (C_l) and drag (C_d) coefficients of the two-dimensional S826 airfoil are validated first followed by the validation of the thrust (C_t), power (C_p) coefficients of the full-scale turbine. Velocity deficit in the wakes on the lee side of the turbine is also compared against the experimental data. To put the current work from a broader perspective, the simulation results are also compared against the previously conducted simulations of the same case albeit with some approximations by other researchers as available in Krogstad and Eriksen (2013).

4.1 Two-dimensional NREL-S826 airfoil aerodynamic characteristics

Two-dimensional analysis of the S826 airfoil at several α extending over attached, mildly separated and stall flow regimes is conducted. The aerodynamic coefficients are compared at Reynolds number of the $Re_{tip} = 10^5$ against the experimental data of Fig. 3 presents the lift and drag coefficients as a function of the angle of attack. The simulations conducted with $k - \omega$ SST exhibit good performance in the attached to the mildly separated regimes. The trend is captured correctly with slight under-prediction of the coefficients. However, the onset of the stall is captured correctly. To determine the qualitative prediction of the flow structure at various α Fig. 4 is plotted. The transition of the flow is exhibited clearly, and the development of flow reversal point is visible in the attached flow region to the transition and stall region. Due to three-dimensional characteristics of the flow in the stall region, BEM is not able to capture the coefficients correctly as the underlying assumption of BEM is based on strictly two-dimensional flow, while the accuracy of our simulations is slightly better. The earlier separation over the suction surface is also noticed near the trailing edge of the airfoil at $\alpha = 12°$. It is associated with the underlying construction of S826 airfoil, which has been designed to increase the lift coefficient at standard operating conditions by increasing the amount of separation over the suction surface.

4.2 Validation and comparison of SMI and MRF

For making a comparison of the accuracy and

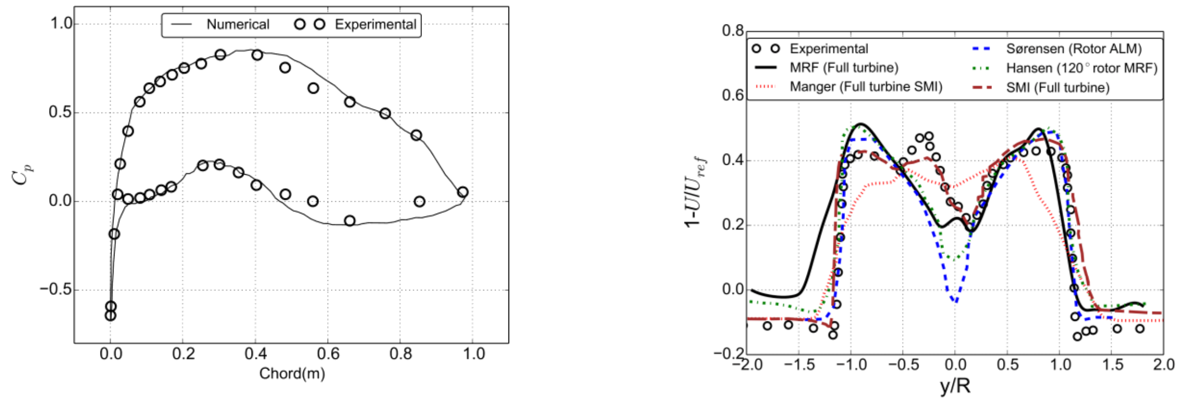

(a) NREL-S826 airfoil (2D aerodynamics): (C_p) (b) NTNU Blind Test: Velocity deficit at x/R = 2

Fig. 5 (a) Validation of the pressure coefficient (C_p) with experimental values for the 2D S826 airfoil cross section. (b) Comparison of the wake velocity deficit (for the case Re = 1×10^5) at the horizontal line located x/R = 2 downstream of the turbine obtained in the present study (multiple reference frames (MRF) and sliding mesh interface (SMI)) with those obtained by numerical simulations and experimental wind tunnel tests reported by Krogstad and Eriksen (2013)

(a) SMI (b) MRF

Fig. 6 NTNU Blind Test: Comparisons of flow patterns obtained by using the sliding mesh interface (SMI) and multiple reference frames (MRF) techniques for handling the rotation of the turbine rotor. The MRF has shown to provide a good assessment of the large features of the flow field, whereas the SMI also captures well the small features present in the flow field

computational efficiency of the SMI and MRF techniques, the experimental case corresponding to λ = 3 is chosen. Since the MRF approach models the time-averaged effects of the flow behavior it is supposed to be faster. This is evident from the fact that an MRF simulation on a 48 core desktop computer with 2.6 GHz Intel(R) Xeon(R) processors took only 72 hours to achieve convergence (Residuals $\leq 10^{-6}$). The SMI approach models the dynamic behavior of the flow and hence was run for a time corresponding to three rotations so that the time-averaged results were statistically meaningful and comparable to the MRF simulation. As expected the SMI simulation was computationally much more demanding taking approximately four weeks on 512 cores with 2.6 GHz Intel(R) Xeon(R) E5-2670 processor on the high-performance supercomputer *Vilje*.

After the comparison of the associated computational time where MRF technique has a clear edge, the focus is shifted to comparing the simulation results against the experimental data. To this end, profiles of the pressure coefficient for α = 0° along the surface of the airfoil and profiles of velocity deficits at different locations and axis are compared in Figs. 5(a) and 5(b) respectively. It is clear from Fig. 5(a) that the simulated profiles on both the upper and lower surface of the airfoil are in good agreement with the experiment. For what concerns velocity deficit, Fig. 5(b) compares horizontal profile (x/R) at a location $y/R = 2$ and $z/R = 0$, on the lee side of the turbine. It can be observed that both the MRF and SMI simulations successfully capture the asymmetry in the profile along with the prediction of a sharp peak. It should be noted that the asymmetry in the profile stems from the rotational effects of the turbine. This is discussed later in this section.

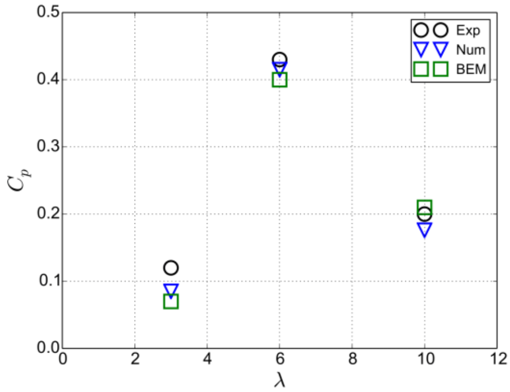

(a) C_p

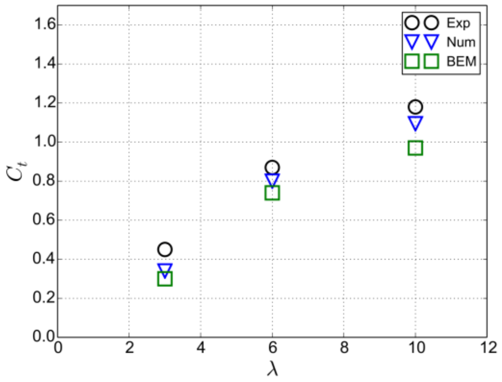

(b) C_t

Fig. 7 NTNU Blind Test: (a) The power coefficient (C_p) and (b) the thrust coefficient (C_t) obtained at three different tip speed ratios λ = 3,6,10 at Re = 1×10^5. The present numerical results (obtained using multiple reference frames (MRF)) are compared with the experimental wind tunnel test (Exp) and Blade Element Model (BEM) data provided by Krogstad and Eriksen (2013)

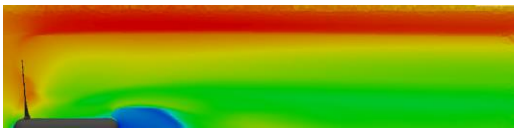

(a) λ = 3

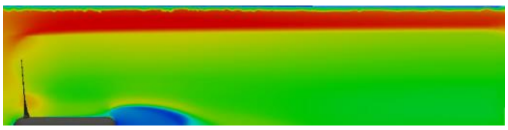

(b) λ = 6

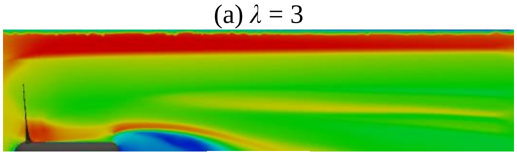

(c) λ = 10

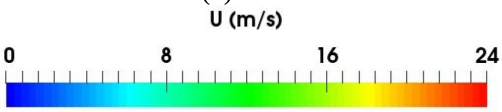

(d) Legend

Fig. 8 NTNU Blind Test: Velocity contours on a plane located in the upper region from the turbine center. Turbine blockage causes flow acceleration between the rotor edge and the wind tunnel walls. At higher tip speed ratios (λ) notice that the rotor operates as a propeller, i.e., by feeding energy into the flow (see figure (c) where a region of high velocities is visible near the root of the blade)

From the figure, it can be observed that our SMI simulation is closest to the experimental results both close to the axis of the turbine and away from it. It should be noted that Manger's simulation setup is closest to ours, but still, it failed to predict the three observed peaks and instead predicts a flatter profile. It appears that the mesh resolution used by Manger was not sufficient to resolve the localized flow features. Sørensen's simulation with the ALM approach produced a good match with the experimental results; however, it was observed to be very inaccurate closer to the axis of the turbine ($-0.5 < y/R < 0.5$). The reason for this can be attributed to the geometrical approximation (ignorance of nacelle and support structure) used in the simulations. Finally, when we compare the prediction of our MRF simulation with that of Hansen's we once again realize the importance of accurately representing the nacelle and using sufficient mesh resolution for resolving the local flow features. The flow around a rotating turbine is dominated by vortex shedding, wake instabilities, and flow unsteadiness and hence SMI approach, which can capture the dynamics is expected to be more accurate than the MRF technique, and this is evident from the Fig. 5(b). The Fig. 6 compares the flow structures in the wakes captured by SMI and MRF techniques and confirms our opinion as mentioned earlier regarding the SMI technique. However, due to the computationally expensive nature of the SMI simulations, it was not feasible to use this technique for conducting sensitivity tests, the kind of which is presented in the following section. Instead, we used a slightly inaccurate but computationally efficient MRF technique.

4.3 Power (C_p) and thrust (C_t) coefficients

Fig. 7 llustrates a comparison of the numerically computed power coefficient ($C_p = \frac{2P}{\rho U_{ref}^3 A_{ref}}$) and thrust

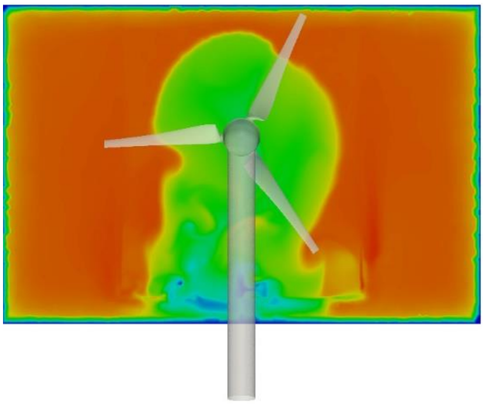

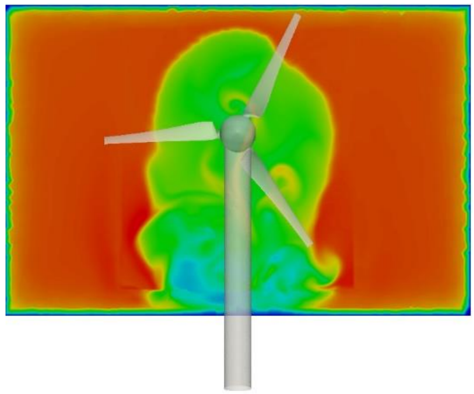

(a) Tip speed ratio λ = 6 (b) Tip speed ratio λ = 10

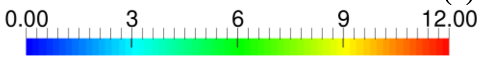

Fig. 9 NTNU Blind Test: Wake velocity structure characterization using multiple reference frame (MRF) on a YZ-plane located at X/R = 6 distance downstream the turbine rotor for tip speed ratios of (a) λ = 6 and (b) λ = 10. The wake is found to be slightly asymmetric across the XZ-plane through the centre of the rotor (units of velocity: m/s)

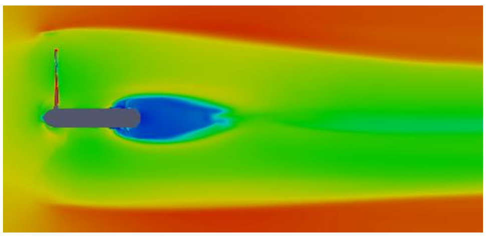

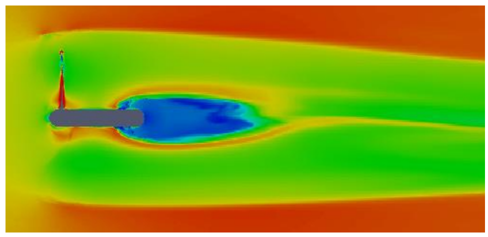

(a) Tip speed ratio λ = 6 (b) Tip speed ratio λ = 10

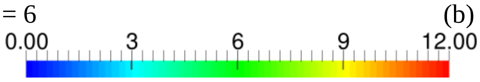

Fig. 10 NTNU Blind Test: Wake velocity structure characterization using multiple reference frame (MRF) at tip speed ratios of (a) λ = 6 and (b) λ = 10 on a XY-plane passing through the rotor centreline (units of velocity: m/s)

coefficient ($C_t = \frac{2T}{\rho U_{ref}^2 A_{ref}}$) of the turbine for three different TSRs. In the expression of power and thrust coefficients, A_{ref}, U_{ref}, ρ, T and P stand for the reference area of the rotor, the reference velocity, the fluid density, the combined thrust and pressure forces on the turbine respectively. As can be seen in the figure, the highest C_p is predicted at the design λ of 6 and this is also in agreement with the experimental observation. Smaller values from BEM in comparison to the CFD is due to the significantly smaller prediction of forces by this method and is also mentioned in the literature by Ronsten (1992).

4.3.1 Flow blockage effect

Objects like wind turbines kept inside a wind tunnel reduce the effective cross-sectional area of the flow and hence results in flow acceleration in some regions of the domain to satisfy the mass conservation. The regions experiencing flow acceleration in the current context is shown in Fig. 8. It is interesting to notice that the blockage effect intensifies with increasing TSR. This can be attributed to the fact that the rotational motion of the blade converts the translational velocity of the flow (in the X direction) into rotation velocity and to conserve the momentum in the X-direction the flow has to accelerate more in regions closer to the wall. In extreme conditions (very high value of λ), the turbine's rotor acts as a solid wall to the incoming flow resulting in high thrust force. This is reflected in the increase of thrust coefficient with λ as reported in Fig. 7.

4.4 Validation of wake profiles

The numerically computed wake deficit (U = 1 - U_{wake}/U_{ref}) profiles over horizontal ($y/R = -3$ to $y/R = +3$) and vertical ($z/R = -2$ to $z/R = +2$) diagonals located at two distinct locations ($x/R = 2, 6$) downstream direction of the turbine are compared against the experimental as well as the simulation results from the other researchers. From the Figs. 11 and 12 it is clear that our MRF simulations outperform the other modelling approaches in terms of accuracy. This is expected since in addition to the explicit representation of the turbine blades we also modelled the nacelle and other support structures as

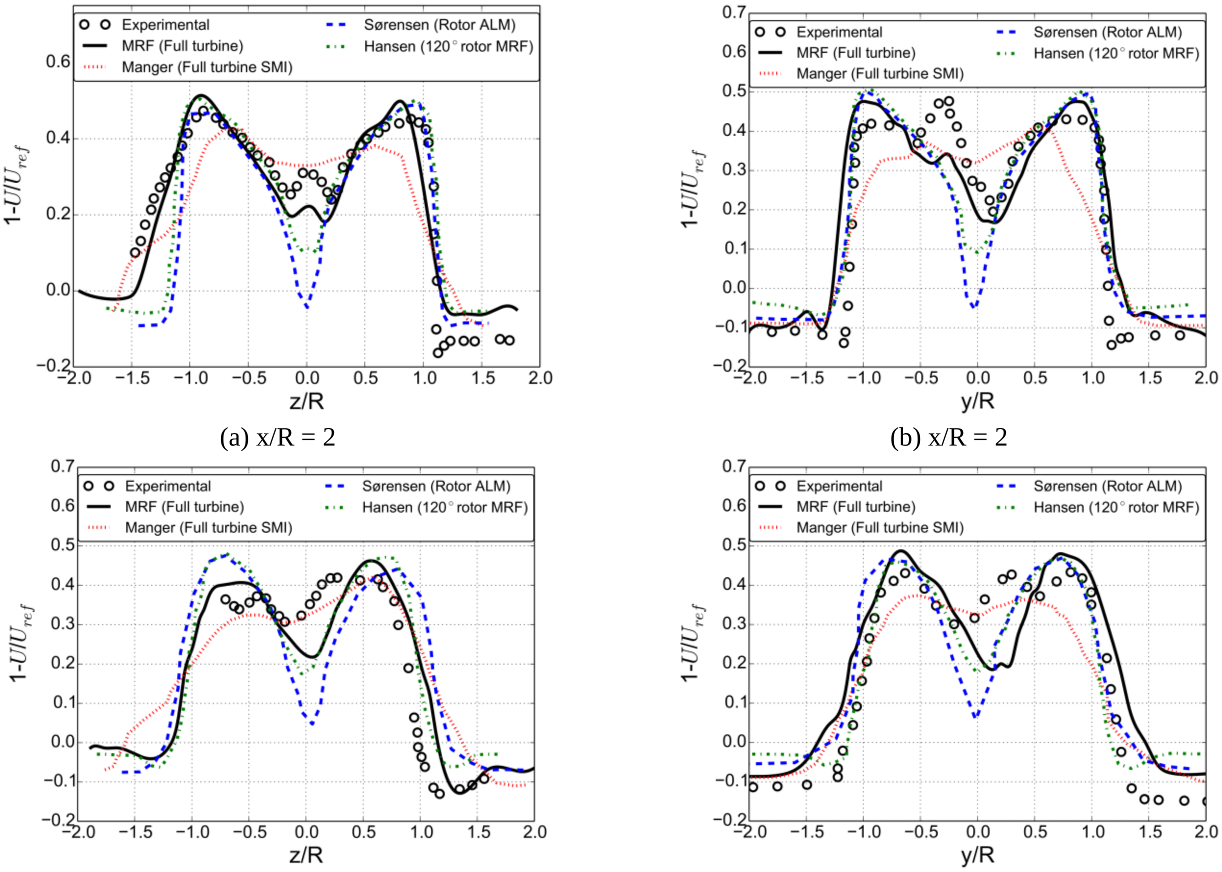

(a) x/R = 2 (b) x/R = 2

(c) x/R = 6 (d) x/R = 6

Fig. 11 NTNU Blind Test: Comparison of the velocity deficit predicted by multiple reference frame (MRF) simulations against the experiments and the similar numerical simulation data reported by Krogstad and Eriksen (2013) extracted on the axis of rotation. The high fidelity MRF simulations are conducted at tip speed ratio of λ = 6 and at Re = 1×10^5

accurately as possible. Moreover, the resolution used for our simulations is much finer compared to other studies. In the next section, we discuss the wake profiles for two distinct TSRs ($\lambda = 6$ and 10).

4.4.1 Wake profiles at $\lambda = 6$

Profiles of wake deficit are presented along vertical and horizontal lines located at two distinct locations ($x/R = 2, 6$) for $\lambda = 6$ are shown in Fig. 11. The observed asymmetry (Figs 9 and 10) in the horizontal profiles can be attributed to the rotational effects of the turbine blade and that in the vertical profiles can be attributed to a combined effect of blade rotation and the wake formation due to the support structure. At $x/R = 2$, three distinct peaks in the profile were reported in the experiment, and our MRF simulation seems to capture them fairly well; however, the exact magnitudes for the second peak is somewhat underpredicted. As one moves further downstream ($x/R = 6$), our MRF simulations start predicting relatively more symmetric profiles. When our results are compared against the results of others, we notice the added value of the explicit representation of nacelle and support structures in the simulation. All the simulations predict the peaks on the extremities accurately; however, they differ a lot closer to the axis of the turbine. While the reason for underprediction in the case of Sørensen and Hansen can be attributed to the neglection of nacelle and support structure in the simulations, Manger's simulation suffers from relatively coarser mesh resolution required to capture the wake physics. The coarse resolution results in numerical dissipation and is exactly this reason that his wake profiles flatten very quickly while moving away from the turbine.

4.4.2 Wake profiles at $\lambda = 10$

A good comparison between the numerical and experimental results at a higher λ is observed. Due to the faster rotation, the turbine starts behaving as a propeller, feeding energy into the wakes, which is apparent from the wake profiles of Fig. 12. This quantitative behavior is also illustrated in the qualitative plots of the velocity contours in Fig. 8 where high velocity (red region) is detected representing a sharp flow acceleration until $x/R = 2$. It creates an area of high velocity; therefore values closer to the reference velocity is observed in the central region of the turbine blade. Whereas, the tip has nearly obstructed the flow and very high-velocity deficit has been observed near

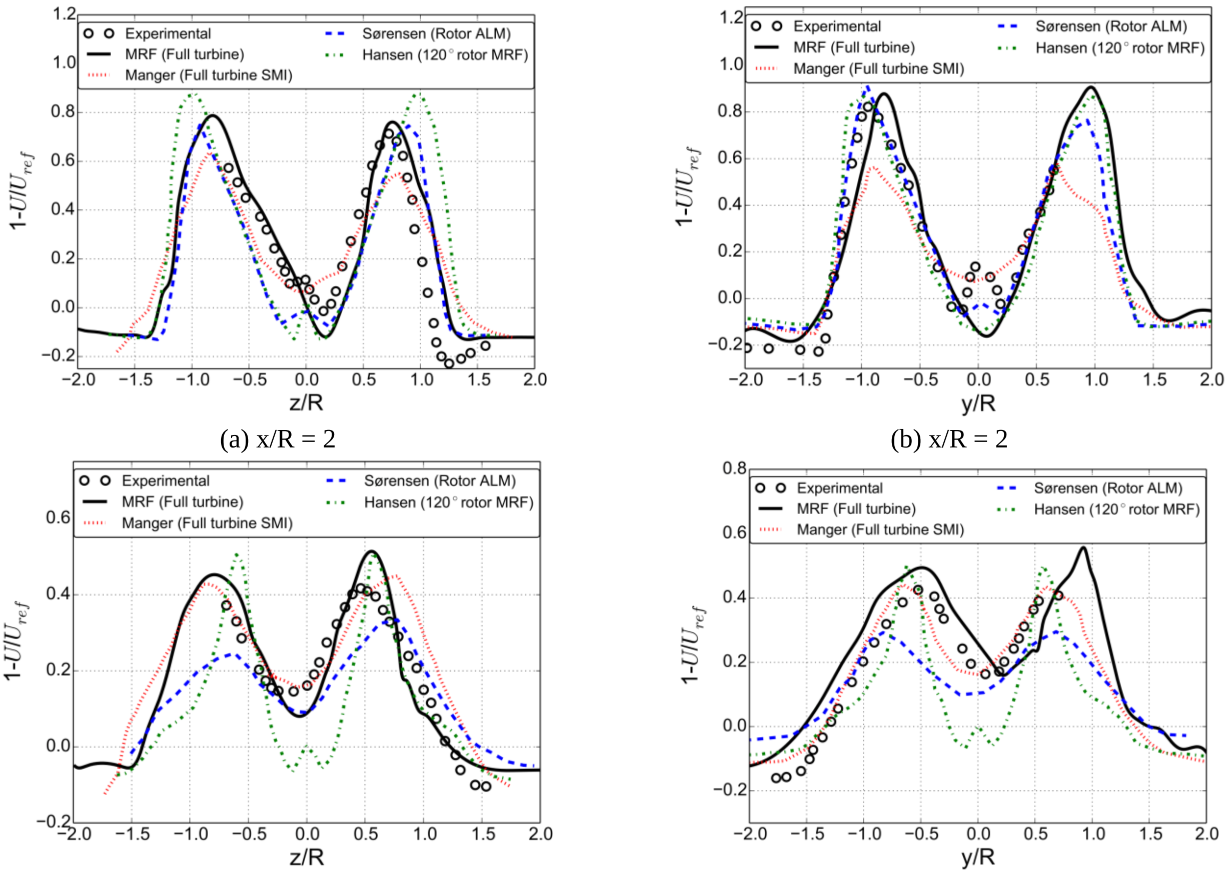

(a) x/R = 2 (b) x/R = 2

(c) x/R = 6 (d) x/R = 6

Fig. 12 NTNU Blind Test: Comparison of the velocity deficit predicted by multiple reference frame (MRF) simulations against the experiments and the similar numerical simulation data reported by Krogstad and Eriksen (2013) extracted on the axis of rotation. The high fidelity MRF simulations are conducted at tip speed ratio of λ = 10 and at Re = 1×10^5

the outer periphery of the rotor which aid to the tunnel blockage. At the next station of $x/R = 6$, it is noticed the sharp gradients present in the wake are reduced by the spanwise diffusion which makes the flow field to become more homogeneous. The peaks of the blockage around the corners of the blades have decreased by approximately a factor of 1.5. Still, the numerical predictions match considerably well with the wake measurements both in the vertical and horizontal directions. Manger predictions match well with MRF at the inner part of the blade at this λ, whereas Hansens wake profiles have shown considerable overprediction at the inner section and have shown a higher increase in the velocity.

5. Conclusions

In this work, the aerodynamic behavior of the S826 airfoil designed by the National Renewable Energy Laboratory (NREL) was first analyzed using two-dimensional numerical simulations using $k - \omega$ Shear Stress Turbulence (SST) Model. Then a three-dimensional model of the turbine including tower and turbine blade (made by circular cross sections close to the nacelle and S826 cross sections elsewhere) was investigated using Sliding Mesh Interface (SMI) and Multiple Reference Frame (MRF) techniques for handling the rotating turbine. The two techniques were validated against wind tunnel experimental data. Both the techniques were found capable of accurately predicting the aerodynamic and wake characteristics of the wind turbine under consideration. Because the SMI technique was computationally demanding, the sensitivity of the turbine's behavior to various tip speed ratio $\lambda = 3, 6, 10$ was evaluated using MRF only. Most important findings of the work are summarized below:

- $k - \omega$ SST turbulence model appears to be a good turbulence model for modeling flow around a 2D airfoil like S826 in attached to mildly separated flow regimes. The onset of the stall is captured correctly.
- SMI and MRF both captures the aerodynamic and wake characteristics of the turbine under consideration for $\lambda = 6$ as observed in the wind tunnel experiment. SMI simulation is ten times more computationally expensive than MRF simulation to produce comparable statistics. The SMI simulations, however, captures the dynamic behaviour as well as the small-scale features of the wake dynamics more accurate than MRF. To our best knowledge our SMI

simulations are the most accurate numerical investigation of the wind tunnel tests carried out over a model wind turbine (known as NTNU Blind Test) at the Norwegian University of Sciences and Technology.

• In the study conducted to evaluate the turbine performance over different tip speed ratios λ, MRF demonstrates the capability of providing fairly correct estimates of the power/thrust coefficient and wake profile patterns in comparison to the wind tunnel experimental and BEM data. The qualitative plots suggest that the turbine was operating in a stalled mode at $\lambda = 3$ with low power and thrust coefficients making larger angle of attack (α) with the oncoming wind. At the design conditions with $\lambda = 6$, highest power coefficient was observed with turbine making optimum angle of attack (α) with the wind. Whereas, at $\lambda = 10$ the highest thrust coefficient was predicted with the blade making an angle of attack (α) in-line with the plane of the rotation of the blade.

• A comparison of our detailed simulation results with that of other previous works highlights the importance of including nacelle and support structures in simulation. The difference was most visible near the hub height and diminishes away from it. For this reason, it can be speculated that the other simplified studies presented in the previous works might be sufficient for power predictions. However, for evaluating structural integrity of a wind turbine as well as wake flow characteristics such simplifications might induce noticeable errors.

With this study, it has been successfully demonstrated the three dimensional MRF and SMI for handling rotation of the turbine are capable of prediction of the wind turbine aerodynamic loading. It is believed that this information at the model scale is crucial and will provide confidence to conduct simulations of megawatt-sized wind turbines, which are currently lacking a wind tunnel experimentation facility. Furthermore, we believe that the present methodology may serve as high-fidelity simulation tool for doing reduced order modelling of wind turbines, see e.g., initial effort by the authors in and . The additional feature of flow visualization associated with the numerical approaches makes them optimal for shaping up the future of wind energy research.

Acknowledgments

The authors acknowledge the financial support from the Norwegian Research Council and the industrial partners of NOWITECH: Norwegian Research Centre for Offshore Wind Technology (Grant No.: 193823/S60) (http://www.nowitech.no), FSI-WT (Grant No.: 216465/E20) (http://www.fsi-wt.no) and OPWIND: Operational Control for Wind Power Plants (Grant No.: 268044/E20). Furthermore, the authors greatly acknowledge the Norwegian Metacenter for computational science (NOTUR-reference number: NN9322K/1589) (www.notur.no) for giving us access to the *Vilje* high-performance computer at the Norwegian University of Science and Technology (NTNU).

References

Alexandros, M. and Chick, J. (2013), "Validation of a CFD model of wind turbine wakes with terrain effects", *J. Wind Eng. Ind. Aerod.*, **123**, 12-29. https://doi.org/10.1016/j.jweia.2013.08.009.

ANSYS Academic Research, 2013. Release 15. ANSYS FLUENT Theory Guide Inc.

Cleaver, D. J., Wang, Z. and Gursul, I. (2010), "Survey of modelling methods for wind turbine wakes and wind farms", *Proceedings of the 48th AIAA Aerospace Sciences Meeting*, Orlando, June.

Crasto, G., Gravdahl, A., Castellani, F. and Piccioni, E. (2012), "Wake modeling with the actuator disc concept", *Energy Procedia*, **24**, 385-392. https://doi.org/10.1016/j.egypro.2012.06.122.

Crespo, A., Hernandez, J. and Frandsen, S. (1999), "Survey of modelling methods for wind turbine wakes and wind farms", *Wind Energy*, **2**(1), 1-24. https://doi.org/10.1002/(SICI)1099-1824(199901/03)2:1<1::AID-WE16>3.0.CO;2-7.

Fonn, E., Brummelen, H.V., Kvamsdal, T. and Rasheed, A. (2019), "Fast divergence-conforming reduced basis methods for steady Navier–Stokes flow", *Comput. Method. Appl. M.*, **346**, 486-512. https://doi.org/10.1016/j.cma.2018.11.038.

Ilhan, A., Bilgili, M. and Sahin, B. (2018), "Analysis of aerodynamic characteristics of 2 MW horizontal axis large wind turbine", *Wind Struct.*, **27**(3), 21-36. https://doi.org/10.12989/was.2018.27.3.187.

Jasak, H. (2009), "Dynamic mesh handling in OpenFoam", *Proceedings of the 47th AIAA Aerospace Sciences Meeting*, Orlando, Florida.

Keerthana, M. and Harikrishna, P. (2017), "Wind tunnel investigations on aerodynamics of a 2:1 rectangular section for various angles of wind incidence", *Wind Struct.*, **25**(3), 301-328. https://doi.org/10.12989/was.2017.25.3.301.

Krogstad, P.A. and Eriksen, P.E. (2013), "Blind test calculations of the performance and wake development for a model wind turbine", *Renew. Energ.*, **50**, 325-333. https://doi.org/10.1016/j.renene.2012.06.044.

Krogstad, P.A. and Sætran, L. (2012), "An experimental and numerical study of the performance of a model turbine", *Wind Energy*, **15**(3), 443-457. https://doi.org/10.1002/we.482.

Krogstad, P.A., Sætran, L. and Adaramola, M.S. (2015), "Blind test 3 calculations of the performance and wake development behind two in-line and offset model wind turbines", *J. Fluids Struct.*, **52**, 65-80. https://doi.org/10.1016/j.jfluidstructs.2014.10.002.

Li, S.W., Hu, Z.Z., Tse, K.T. and Weerasuriya, A.U. (2016), "Wind direction field under the influence of topography: part II: CFD investigations", *Wind Struct.*, **22**(2), 477-501. : http://dx.doi.org/10.12989/was.2016.22.4.477.

Luhur, M.R., Manganhar, A.L., Solangi, K.H., Jakhrani, A.Q., Mukwana, K.C. and Samo, S.R. (2016), "A review of the state-of-the-art in aerodynamic performance of horizontal axis wind turbine", *Wind Struct.*, **22**(1), 1-16. http://dx.doi.org/10.12989/was.2016.22.1.001.

Martinez Tossas, L.A., Churchfield, M.J. and Leonardi, S. (2015), "Large eddy simulations of the flow past wind turbines: actuator line and disk modeling", *Wind Energy*, **18**(6), 1047-1060. https://doi.org/10.1002/we.1747.

Mo, J.O., Choudhry, A., Arjomandi, M. and Lee, Y.H. (2013), "Large eddy simulation of the wind turbine wake characteristics in the numerical wind tunnel model", *J. Wind Eng. Ind. Aerod.*, **112**, 11-24. https://doi.org/10.1016/j.jweia.2012.09.002.

Nordanger, K., Holdahl, R., Kvamsdal, T., Kvarving, A.M. and

Rasheed, A. (2015), "Simulation of airflow past a 2D NACA0015 airfoil using an isogeometric incompressible Navier-Stokes solver with the Spalart-Allmaras turbulence model", *Comput. Method. Appl. M.*, **290**, 183-208. https://doi.org/10.1016/j.cma.2015.02.030.

Nordanger, K., Holdahl, R., Kvarving, A.M., Rasheed, A. and Kvamsdal, T. (2015), "Implementation and comparison of three isogeometric Navier-Stokes solvers applied to simulation of flow past a fixed 2D NACA0012 airfoil at high Reynolds number", *Comput. Method. Appl. M.*, **284**, 664-688. https://doi.org/10.1016/j.cma.2014.10.033.

Ozdogan, M., Sungur, B., Namli, L. and Durmus, A. (2017), "Comparative study of turbulent flow around a bluff body by using two and three-dimensional CFD", *Wind Struct.*, **25**(6), 537-549. https://doi.org/10.12989/was.2017.25.6.537.

Ronsten, G. (1992), "Static pressure measurements on a rotating and a non-rotating 2.375 m wind turbine blade. Comparison with 2D calculations", *J. Wind Eng. Ind. Aerod.*, **39**(1-3), 105-118. https://doi.org/10.1016/0167-6105(92)90537-K.

Sanderse, B., van der Pijl, S. amd Koren, B. (2011), "Review of computational fluid dynamics for wind turbine wake aerodynamics", *Wind Energy*, **14**(7), 799-819. https://doi.org/10.1002/we.458.

Siddiqui, M.S., Fonn, E., Kvamsdal, T. and Rasheed, A. (2019), "Finite-volume high-fidelity simulation combined with finite-element-based reduced-order modeling of incompressible flow problems", *Energies*, **12**(7), 1271-1293. https://doi.org/10.3390/en12071271.

Siddiqui, M.S., Rasheed, A., Kvamsdal, T. and Kvamsdal, T. (2017), "Quasi-static and dynamic numerical modeling of full scale NREL 5MW wind turbine", *Energy Procedia*, **137**, 460-467. https://doi.org/10.1016/j.egypro.2017.10.370.

Siddiqui, M.S., Rasheed, A., Kvamsdal, T. and Tabib, M. (2015), "Effect of turbulence intensity on the performance of an offshore vertical axis wind turbine", *Energy Procedia*, **80**, 312-320. https://doi.org/10.1016/j.egypro.2015.11.435.

Siddiqui, M.S., Rasheed, A., Tabib, M. and Kvamsdal, T. (2019), "Numerical investigation of modeling frameworks and geometric approximations on NREL 5 MW wind turbine", *Renew. Energ.*, **132**, 1058-1075. https://doi.org/10.1016/j.renene.2018.07.062.

Snel, H., Schepers, J.G. and Montgomerie, B. (2007), "The MEXICO project (model experiments in controlled conditions): The database and first results of data processing and interpretation", *J. Physics*, **75**, 012014.

Somers, D.M. (2005), "The S825 and S826 airfoils", *Techincal Report NREL/SR-500-36344*, National Renewable Energy Laboratory, CO, USA.

Sørensen, J., Shen, W.Z. and Munduate, X. (1998), "Analysis of wake states by a full-field actuator disc model", *Wind Energy*, **1**, 73-88. https://doi.org/10.1002/(SICI)1099-1824(199812)1:2<73::AID-WE12>3.0.CO;2-L.

Sørensen, N.N., Bechmann, A., Boudreault, L.E., Koblitz, T. and Sogachev, (2013), "A CFD applications in wind energy using RANS",*CFD for atmospheric flows and wind engineering, von Karman Institute for Fluid Dynamics*, Lecture Series, No. 2013-02.

Sørensen, N.N., Michelsen, J.A. and Schreck, S. (2002), "Navier-Stokes predictions of the NREL phase VI rotor in the NASA Ames 80ft x 120ft wind tunnel", *Wind Energy*, **5**, 151-169. DOI: 10.1002/we.64.

Stevens, R.J., Tossas, L.A.M. and Meneveau, C. (2018), "Comparison of wind farm large eddy simulations using actuator disk and actuator line models with wind tunnel experiments", *Renew. Energ.*, **116**, 470-478. https://doi.org/10.1016/j.renene.2017.08.072.

Troldborg, N., Sørensen, J.N. and Mikkelsen, R. (2007), "Actuator line simulation of wake of wind turbine operating in turbulent inflow", *J. Physics*, **75**, 012063.

Troldborg, N., Zahle, F. and Sørensen, N.N. (2015), "Simulation of a MW rotor equipped with vortex generators using CFD and an actuator shape model", *Proceedings of the 53rd AIAA Aerospace Sciences Meeting*, Kissimmee, Florida.

Wilcox, D. (1994), "Simulation of transition with a two-equation turbulence model", *AIAA J.*, **32**, 247-255.

Yang, H., Shen, W., Xu, H., Hong, Z. and Liu, C. (2014), "Prediction of the wind turbine performance by using BEM with airfoil data extracted from CFD", *Renew. Energ*, **70**, 107-115. https://doi.org/10.1016/j.renene.2014.05.002

Zhang, Y., Gillebaart, T., van Zuijlen, A., van Bussel, G. and Bijl, H. (2017), "Experimental and numerical investigations of aerodynamic loads and 3D flow over non-rotating MEXICO blades", *Wind Energy*, **20**(4), 585-600. https://doi.org/10.1002/we.2025.

Zhong, H., Du, P., Tang, F. and Wang, L. (2015), "Lagrangian dynamic large-eddy simulation of wind turbine near wakes combined with an actuator line method", *Appl. Energy*, **144**, 224-233. https://doi.org/10.1016/j.apenergy.2015.01.082.

Zhong, H., Du, P., Tang, F. and Wang, L. (2015), "Lagrangian dynamic large-eddy simulation of wind turbine near wakes combined with an actuator line method", *Appl. Energy*, **144**, 224-233. https://doi.org/10.1016/j.apenergy.2015.01.082.

FR